Bažant, Z.P., and Burrow, M. C. (1980). "Confinement effect in flexural ductility of concrete: Three dimensional analysis." *Materials and Structures* (RILEM, Paris), 13, 296–308.

Confinement effect in flexural ductility of concrete: three-dimensional analysis

Z. P. Bažant (1), M. C. Burrow (2)

To study the effect of the transverse stress and strain distribution and steel ties (stirrups) upon the ultimate bending moment and bending ductility, a three-dimensional finite element analysis of a cross section slice is carried out. The slice consists of a layer of eight-node isoparametric elements, whose axial displacements are constrained so that the cross sections remain planar but not orthogonal. This allows interpreting the results in terms of curvature, bending moment, axial force and shear force. Each element within the layer is allowed to independently undergo cracking when its tensile strength limit is exceeded, and the incremental inelastic stiffness matrix of the cracked material is derived. The inelastic behavior of uncracked concrete or concrete between the cracks is modeled by the previously published endochronic theory, which allows representing the inelastic dilatancy due to shear, the hydrostatic pressure sensitivity, and the strain-softening (decrease of stress at increasing strain). The use of a constitutive relation that is capable of describing these effects is essential, since the dilatancy of concrete is opposed by ties which thus produce hydrostatic pressure in concrete thereby increasing its ductility. Transverse reinforcement is modeled either as reinforcement smeared throughout an element or as a steel bar connecting the nodes. Special measures are taken to eliminate spurious shear effects in the finite element model. A computer program to calculate the moment-curvature diagram of a given beam has been written using the incremental loading procedure. The calculated results compare satisfactorily with the available published test data on the effect of tie spacing upon the moment-curvature diagrams and flexural ductility.

NOTATIONS

$\mathbf{C}$, $\mathbf{D}$,	stiffness matrix (moduli) of concrete and of element material;
$\mathbf{f}$, $\mathbf{f}''$,	column matrices of nodal forces and inelastic nodal forces;
k,	curvature;
$\mathbf{K}$,	element stiffness matrix;
M, N,	bending moment and normal force;
S_{ij}'',	inelastic stresses in concrete;
$\mathbf{q}$,	column matrix of nodal displacements;
$\mathbf{R}$,	rotation transformation matrix for crack plane [equation (29)];
$\mathbf{T}$,	transformation matrix for planar cross section constraint [equation (6)];
u, v, w,	cartesian displacement (u = axial);
x, y, z,	cartesian coordinates (x = axial);
ε_0,	normal strain at beam axis;
ε_{ij}, $\boldsymbol{\varepsilon}$,	small strains and their column matrix;
σ_{ij}, $\boldsymbol{\sigma}$,	stresses and their column matrix;
$\boldsymbol{\sigma}''$,	column matrix of inelastic stresses.

OBJECTIVE

Although the mechanics of bending of reinforced concrete beams is quite well understood, certain properties are at present known only empirically, and therefore incompletely. These are the properties that can be modelled only with the help of a triaxial nonlinear constitutive relation of concrete. One such property is the effect of transverse ties or stirrups on bending, as distinct from shear. As far as bending is concerned, the code requirements for the necessary amount of ties are purely empirical.

(1) Professor of Civil Engng., Northwestern University, Evanston, Illinois 60201.

(2) Engineer, Skidmore, Owings and Merrill, Chicago, Illinois; formerly Graduate Research Assistant, Northwestern University, Evanston, Illinois.

0025-5432/1980/299/$ 5.00/© BORDAS-DUNOD

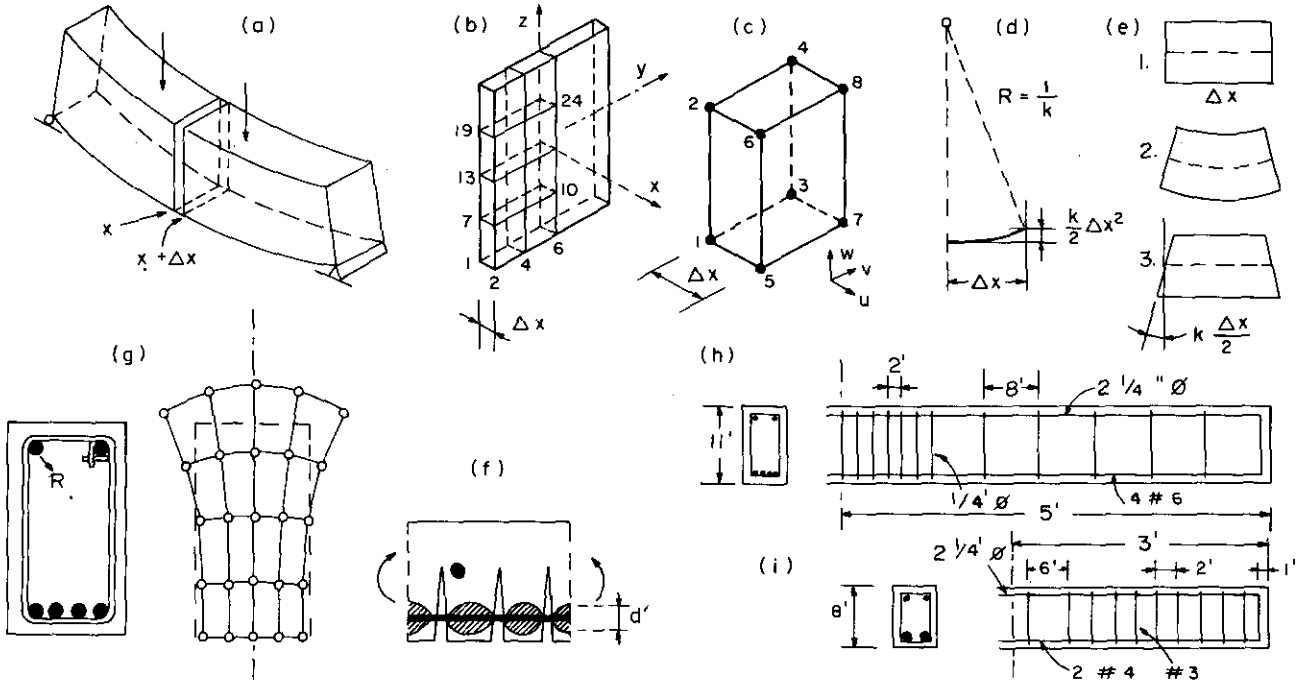

Fig. 1. – Cross section slice and finite elements (*a–c*); deformation diagrams (*d–f*), and reinforcement (*g, h, i*).

The effect of ties is to provide a confinement of concrete. The inelastic dilatancy due to deviatoric strains in the compression zone induces tension in the ties concrete, thereby greatly raising concrete strength and ductility. Obviously, a good nonlinear triaxial ductility. Obviously, a good non linear triaxial constitutive law is requisite for analyzing effects of this sort, and one such constitutive relation has recently become available in the form of endochronic theory ([2], [3], [5], [9]). The objective of this study is to show how this theory can be utilized for analyzing the effect of ties on bending. The mathematical model developed can, however, be also used in a multitude of further studies of the effect of various design parameters upon the ultimate load behavior.

The present study represents a sequel to a previous work [4] in which the endochronic theory was utilized to analyze the behavior of beams under cyclic loading with a two-dimensional model in which the cross sections were subdivided in layers, neglecting effects in the lateral dimension. In that study the effect of ties on ductility under cyclic loading was found to be rather significant. However, the two-dimensional simplification, in which the cross-section behavior was limited to vertical strains in the cross section plane, was certainly a questionable point which precluded seeing the effect of a horizontal segment of a stirrup, or the effect of a closed versus an open form of a stirrup, or the effect of stress concentrations due to the force exerted by a stirrup corner on concrete, etc. The present study attempts a step toward a rational analysis of such effects. When the three-dimensional modeling, coupled with a realistic nonlinear triaxial constitutive relation for concrete, including cracking, becomes mature, it will be possible to run calculations of hundreds of combinations of various design parameters, the cost of which would be prohibitive with a purely experimental approach.

To be able to interpret the results in terms of bending moment and curvature, we will limit our analysis to a cross section slice (*fig.* 1 *a, b*), which we will subdivide by three-dimensional eight-node elements (*fig.* 1 *b, c*) to account for the cross-section deformation (*fig.* 1 *g*).

FINITE ELEMENT ANALYSIS OF CROSS SLICE OF BEAM

In view of the constraint that the cross sections must remain plane, it suffices to analyse a single cross section. However, for the purpose of utilizing the finite element formalism, it is more convenient to imagine a thin cross slice of thickness Δx, limited by cross sections at x and $x+\Delta x$ (*fig.* 1 *a*); x is the longitudinal axis of the beam, which may (but need not) be located at the elastic centroid of the cross section. The other cartesian coordinate axes y and z point in the lateral and vertical directions, respectively, and plane (xz) is the plane of bending.

In the classical problem of bending, we seek the relationship of bending moment M, axial (normal) force N and shear force V to the curvature k, and (normal) strain ε_0, and shear strain γ_{xz}. In reality, however, this number of variables is not sufficient because deformations and stresses in cross section plane (yz) may have a great influence. Their analysis will be our primary interest, and for this purpose we will subdivide the cross section slice by three-dimensional finite elements (*fig.* 1 *b*). These are chosen as eight-node isoparametric elements [26], whose displacements are

assumed to vary linearly between the nodes (*fig.* 1 *c*). In case of orthogonal shape and homogeneous elastic properties, explicit expressions for the stiffness matrix are available [20].

For a small loading increment, the constitutive relation of the material may be considered in the quasi-linear form

$$\Delta\boldsymbol{\sigma}+\Delta\boldsymbol{\sigma}''=\mathbf{D}\,\Delta\boldsymbol{\varepsilon}, \tag{1}$$

in which $\boldsymbol{\varepsilon}=(6\times 1)$ column matrix of the small strain components $=(\varepsilon_x, \varepsilon_y, \varepsilon_z, \gamma_{xy}, \gamma_{yz}, \gamma_{zx})^T$, where superscript T denotes a transpose, $\boldsymbol{\sigma}=(6\times 1)$ column matrix of the associated stress components, $\Delta\boldsymbol{\sigma}''=$known (6×1) column matrix of the inelastic stress increments, $\mathbf{D}=$incremental (6×6) matrix of elastic moduli.

As is well known, the application of the virtual work principle leads to the variational equilibrium equation

$$\Sigma_{el}\left\{\delta\mathbf{q}^T\,\Delta\mathbf{f}-\int_V \delta\boldsymbol{\varepsilon}^T\,(\mathbf{D}\,\Delta\boldsymbol{\varepsilon}-\Delta\boldsymbol{\sigma}'')\,\mathrm{d}V\right\}$$
$$=\Sigma_{el}\,\delta\mathbf{q}^T\,(\Delta\mathbf{f}+\Delta\mathbf{f}''-\mathbf{K}\,\Delta\mathbf{q})=0, \tag{2}$$

with

$$\mathbf{K}=\int_V \mathbf{B}^T\,\mathbf{D}\mathbf{B}\,\mathrm{d}V, \qquad \Delta\mathbf{f}''=\int\mathbf{B}^T\,\Delta\boldsymbol{\sigma}''\,\mathrm{d}V, \tag{3}$$

which must hold for any kinematically admissible variations $\delta\mathbf{q}^T$. Here

$$\mathbf{q}=(u_1, v_1, w_1, \ldots, u_4, v_4, w_4)^T$$

is the (24×1) column matrix of cartesian displacements u_i, v_i, w_i (in x, y, z directions) of element nodes $i=1, 2, \ldots, 8$ (*fig.* 1 *c*), $\mathbf{f}=(24\times 1)$ column matrix of associated nodal forces f_{x_i}, f_{y_i}, f_{z_i} in the x, y, z directions, $\Delta\mathbf{f}''=(24\times 1)$ column matrix of equivalent inelastic nodal force increments, $\mathbf{K}=(24\times 24)$ incremental stiffness matrix of the element, $V=$volume of the element; Σ_{el} indicates the superposition of contributions from all elements of the system; and $\mathbf{B}=(6\times 24)$ geometrical matrix defined by the relation $\boldsymbol{\varepsilon}=\mathbf{B}\,\mathbf{q}$.

Stiffness matrix $\mathbf{K}$ as well as incremental inelastic force matrix $\Delta\mathbf{f}''$ may be evaluated by numerical integration, with two integration points in each direction.

To relate the finite element analysis to the mechanics of bending, we must introduce the constraint that the cross sections forming the faces of the slice must remain planar. We do not require them, however, to remain normal to the deflected neutral axis, i. e. we assume a higher-order bending theory (Timoshenko beam). Let the face x of the slice contain axes y and z. For this face the constraint is expressed by

$$u_i=0 \qquad (i=1, 2, 3, 4), \tag{4}$$

where nodes $i=1, 2, 3, 4$ of each element at $x=$Const. For the opposite face of the slice, which is located at $x+\Delta x$ and contains the nodes $i=5, 6, 7, 8$ of each element (*fig.* 1 *b*), the constraint leads to the relations

$$u_{i+4}=(\varepsilon_0-kz_i)\,\Delta x, \tag{5a}$$

$$v_{i+4}=v_i \qquad (i=1, 2, 3, 4), \tag{5b}$$

$$w_{i+4}=w_i+\gamma_{xz}\,\Delta x+\frac{k}{2}(\Delta x)^2, \tag{5c}$$

in which $\Delta x=$thickness of the slice, $z_i=$vertical z-coordinate common to nodes i and $i+4$, $k=$bending curvature of the beam, $\varepsilon_0=$longitudinal normal strain in the beam axis, and $\gamma_{xz}=$transverse shear strain in the (xz) plane, assumed to be constant throughout the cross section. The term $(\Delta x)^2\,k/2$ follows from the geometrical sketch in figure 1 *d*.

It is expedient to form the constrained displacement matrix of the element,

$$\mathbf{q}^*=(k, \varepsilon_0, \gamma_{xz}, v_1, w_1, \ldots, v_4, w_4),$$

which represents an (11×1) column matrix. Equations (4) and (5), which introduce the bending constraints, may now be rewritten in the matrix form:

$$\mathbf{q}=\mathbf{T}\,\mathbf{q}^*, \tag{6}$$

in which $\mathbf{T}=$ a (24×11) matrix of inverse transformation from $\mathbf{q}^*$ to $\mathbf{q}$ (*see* appendix I). Substituting this relation into equation (2), and noting that $(\mathbf{T}\,\mathbf{q}^*)^T=\mathbf{q}^{*T}\,\mathbf{T}^T$, we obtain the variational equilibrium equation

$$\Sigma_{el}\,\delta\,\mathbf{q}^{*T}\,\mathbf{T}^T\,(\Delta\mathbf{f}+\Delta\mathbf{f}''-\mathbf{K}\mathbf{T}\,\Delta\mathbf{q}^*)=0. \tag{7}$$

Since it must hold for any kinematically admissible variation $\delta\mathbf{q}^*$, we have the matrix equilibrium equation

$$\Delta\hat{\mathbf{f}}+\Delta\hat{\mathbf{f}}''=\hat{\mathbf{K}}\,\Delta\hat{\mathbf{q}}^*, \tag{8}$$

where hat denotes assembled transformed matrices for the entire system, i. e.,

$$\hat{\mathbf{K}}=\Sigma_{el}\,\mathbf{K}^*=\Sigma_{el}\,\mathbf{T}^T\,\mathbf{K}\mathbf{T}, \tag{9}$$

$$\Delta\hat{\mathbf{f}}=\Sigma_{el}\,\Delta\mathbf{f}^*=\Sigma_{el}\,\mathbf{T}^T\,\Delta\mathbf{f}, \tag{10}$$

$$\Delta\hat{\mathbf{f}}''=\Sigma_{el}\,\Delta\mathbf{f}''^*=\Sigma_{el}\,\mathbf{T}^T\,\Delta\mathbf{f}''. \tag{11}$$

Here $\mathbf{K}^*=(11\times 11)$ transformed incremental stiffness matrices of the elements, $\Delta\mathbf{f}^*=$matrix of transformed applied nodal force increments of an element, $\Delta\mathbf{f}''^*=$matrix of transformed known inelastic nodal force increments of an element. Matrix $\Delta\hat{\mathbf{f}}^*$ includes as their first three components the generalized forces that do work on k, ε_0 and γ_{xz}, i. e., bending moment M, axial (normal) force N, and shear force V.

The matrix products indicated in equations (9)-(11) are unnecessarily costly to perform by the computer. Therefore, these products have been evaluated and programmed in terms of matrix elements.

Since we restricted ourselves to bending in the plane (xz), the shear stresses τ_{xy} must be zero. For the finite element model this means that the forces in the y-direction applied at all nodes from one side of cross section upon the other side must be zero. By treating in the finite element program the face of the slice as a free

surface with no load, this condition is, indeed, automatically satisfied.

One question with respect to the element choice remains to be answered. In longitudinal sections, the 8-node isoparametric element is equivalent to a 4-node quadrilateral (*fig.* 1 *e*), which is known to be excessively stiff in case of bending of slender beams because of a phenomenon of spurious shear stiffness. Is it possible to circumvent this drawback?

In fact, it is, and to show it, consider the case of a single element in pure bending illustrated in figure 1 *e*. The actual deformation involves no shear strains (2 in the figure 1 *e*), whereas the assumed linear interpolation functions do involve shear strains γ_{xz} for the same nodal displacements (3 in the figure 1 *e*); $\gamma_{xz}=k\bar{x}$ where $\bar{x}=x$ minus the value of x at element midlength. The corresponding energy U_s of shear strains is $\Delta y\,\Delta z\int G\,\gamma_{xz}^2\,d\bar{x}/2$ from $\bar{x}=-\Delta x/2$ to $\bar{x}=\Delta x/2$, which yields $U_s=G\,k^2\,\Delta x^3\,\Delta y\,\Delta z/24$. The energy of bending at zero extension ε_x at element midheight is $U_b=EI\,k^2\,\Delta x/2$ where $E=$Young's modulus, $I=\Delta y\,\Delta z^3/12$. Thus, the ratio of spurious shear energy to the bending energy is

$$\frac{U_s}{U_b}=\frac{G}{E}\left(\frac{\Delta x}{\Delta z}\right)^2. \tag{12}$$

Consequently, the effect of spurious shear due to pure bending becomes negligible if Δx is small enough. In practical calculations, Δx was considered to be 0.0001 of the smallest cross section dimension, by which the spurious shear was completely eliminated. One might wonder whether such a thin and flat shape of the three-dimensional elements is not a source of another error; but this is not a problem in the presence of bending constraints. Note also that for a very small Δx the term $(\Delta x)^2\,k/2$ in equation (5 *c*) becomes negligible compared to the terms linear in Δx and may be dropped.

There exists another well known method to eliminate spurious shear. It is the "reduced" numerical integration of element stiffness, which consists in evaluating the shear stiffness of the element solely from the mid-element shear strain values. This method has been also programmed, and gave for non-negligible Δx the same results as the foregoing method.

PROPERTIES OF PLAIN UNCRACKED CONCRETE

Although stirrups or ties have almost no effect on service deformations and little effect on failure loads, they strongly affect ductility, as is well known from experiments as well as recent theoretical calculations [4]. Therefore, it would be impossible to theoretically analyze the effect of stirrups without a triaxial constitutive relation that is correct throughout the maximum stress region and well into the strain-softening range. Moreover, since the effect of stirrups or ties stems mainly from the hydrostatic pressure induced in concrete by the resistance of stirrups to inelastic volume dilatancy, the constitutive relation must reflect these properties correctly.

At present there exist two constitutive models that have the required scope. They are the endochronic theory, which has already appeared in three successive versions of improving scope and accuracy ([2], [3], [5], [6], [7], [9]) and the recent plastic-fracturing theory ([6], [8]). The second version of the endochronic theory ([3], [5]) was used in this study, for the last one ([9], [7]) as well as the plastic-fracturing theory [8] have been completed only after concluding the calculations. Time effects and shrinkage are excluded, in which case the constitutive relation has the incremental form ([3], [5]):

$$\left.\begin{aligned}\Delta e_{ij}&=\frac{\Delta s_{ij}}{2G(\lambda)}+\Delta e''_{ij},\\ \Delta e''_{ij}&=\frac{s_{ij}}{2G(\lambda)}\,\Delta\zeta,\end{aligned}\right\} \tag{13}$$

$$\left.\begin{aligned}\Delta\varepsilon&=\frac{\Delta\sigma}{3K(\lambda)}+\Delta\varepsilon'',\\ \Delta\varepsilon''&=\Delta\lambda+\Delta\lambda'+\frac{\sigma}{3K(\lambda)}\,\Delta\zeta',\end{aligned}\right\} \tag{14}$$

$$\left.\begin{aligned}\Delta\zeta&=\frac{\Delta\eta}{f(\eta,\boldsymbol{\varepsilon},\boldsymbol{\sigma})},\\ \Delta\eta&=F(\boldsymbol{\varepsilon},\boldsymbol{\sigma})\,\Delta\xi,\\ \Delta\xi&=\sqrt{\frac{1}{2}\,\Delta e_{km}\,\Delta e_{km}},\end{aligned}\right\} \tag{15}$$

$$\left.\begin{aligned}\Delta\zeta'&=\frac{\Delta\eta'}{h(\eta')},\\ \Delta\eta'&=H(\boldsymbol{\sigma})\,\Delta\xi',\\ \Delta\xi'&=\left|\Delta\varepsilon_{11}+\Delta\varepsilon_{22}+\Delta\varepsilon_{33}\right|,\end{aligned}\right\} \tag{16}$$

$$\left.\begin{aligned}\Delta\lambda&=l(\lambda)\,L(\lambda,\boldsymbol{\varepsilon},\boldsymbol{\sigma})\,\Delta\xi,\\ \Delta\lambda'&=l'(\lambda')\,L'(\lambda',\boldsymbol{\varepsilon},\boldsymbol{\sigma})\,\Delta\xi,\end{aligned}\right\} \tag{17}$$

in which Δ refers to an increment over the loading step, $e_{ij}=\varepsilon_{ij}-\delta_{ij}\,\varepsilon=$strain deviator in cartesian coordinates $x_1=x, x_2=y, x_3=z$ referred to by latin subscripts (e. g., $i=1, 2, 3$), $\varepsilon_{ij}=$components of small strain tensor $\boldsymbol{\varepsilon}$, $\delta_{ij}=$Kronecker delta, $\varepsilon=\varepsilon_{kk}/3=$volumetric strain (repeated subscript implies summation), $s_{ij}=\sigma_{ij}-\delta_{ij}\,\sigma=$stress deviator, $\sigma=$components of stress tensor $\boldsymbol{\sigma}$, $\sigma=\sigma_{kk}/3=$mean normal stress, $G, K=$shear and bulk modulus, $\lambda=$inelastic dilatancy, $\lambda'=$shear compaction, $\zeta=$deviatoric intrinsic time, $\xi=$deviatoric path length, $\zeta'=$volumetric intrinsic time, $\xi'=$volumetric path length. Functions F, f, H, h, L, l, L', l', $G(\lambda)$, $K(\lambda)$ define material properties and are given in references [3] and [5] as functions of concrete strength f'_c.

Equations (13) and (14) can be recast in the form

$$\Delta\boldsymbol{\sigma}+\Delta\mathbf{S}''=\mathbf{C}\,\Delta\boldsymbol{\varepsilon}, \tag{18}$$

describing the effects of cracks on inelastic strains, do not seem to have been given before.

In summary, the incremental inelastic stress-strain relation for concrete that is cracked in planes normal to the x_1^* axis is, according to equations (22)-(26):

$$\Delta\boldsymbol{\sigma}^* + \Delta\bar{\mathbf{S}}'' = \bar{\mathbf{C}}\,\Delta\boldsymbol{\varepsilon}^*, \tag{27}$$

where $\bar{\mathbf{C}}$ is a (6×6) matrix whose first row as well as column is zero, $\bar{C}_{1k}=\bar{C}_{k1}=0$ for all k. The elements of $\bar{\mathbf{C}}$ other than those given by equations (24) and (26) are also zero.

Cracking of concrete in a second or third direction can be dealt with similarly, but is not needed for the present practical calculations.

Having established the incremental stress-strain relation in crack coordinates, we must transform it back to structural coordinates x_i. Thus, equation (27) yields:

$$\Delta\boldsymbol{\sigma} + \Delta\boldsymbol{\sigma}'' = \mathbf{D}^c\,\Delta\boldsymbol{\varepsilon} \quad \text{(concrete only)}, \tag{28}$$

in which

$$\Delta\boldsymbol{\sigma}'' = \mathbf{R}^T\,\Delta\bar{\mathbf{S}}'', \qquad \mathbf{D}^c = \mathbf{R}^T\bar{\mathbf{C}}\mathbf{R}, \tag{29}$$

If there are no cracks, then of course $\mathbf{D}^c=\mathbf{C}$, $\Delta\boldsymbol{\sigma}''=\Delta\mathbf{S}''$.

In the preceding study [4], the inelastic stress increments were assumed as $\Delta\mathbf{S}''$ rather than $\Delta\boldsymbol{\sigma}''$. The present derivation shows that the use of $\Delta\boldsymbol{\sigma}''$ is, however, more reasonable. Nevertheless, the values of $\Delta\boldsymbol{\sigma}''$ for cracked concrete are usually negligible, unless there are significant compression stresses parallel to the crack.

During the loading step in which cracks form, the stress $\sigma_1=\sigma_{11}^*$ which existed at the beginning of the loading step must be cancelled, which is accomplished by increasing $\Delta\bar{S}_{11}''$ for this step by $-\sigma_1$ before $\Delta\boldsymbol{\sigma}''$ is calculated from equation (29).

In absence of transverse shears γ_{xy}, γ_{xz} in the beam, cracks are always either normal or parallel to axis x. If transverse shears are present, cracks in any element can have any three-dimensional direction.

The material properties as well as cracking have been determined independently for each integration point of the element.

Finally, it is appropriate to replace the transverse vertical shear stiffness D_{44}^c with βD_{44}^c where β is Timoshenko's shear correction coefficient known from elastic beam deflection calculations. For rectangular cross sections considered herein, $\beta=1.2$. Without this correction, the shear deflection obtained for an elastic material would not agree with observations. The correction is, however, not too important, because in slender beams the shear strain contributes to deflection only little.

Crack closing needs not be discussed because only monotonic loading is considered in the examples.

STIFFNESS DUE TO REINFORCEMENT

A rather convenient way to represent reinforcement is to assume it to be "smeared" (continuously distributed) throughout the element or its portion. In our case, the element may be subdivided in eight portions, each corresponding to one integration point, and the total reinforcement may be apportioned by requiring that the static moments of reinforcement areas be preserved. Thus, the reinforcement may be characterized by percentages p_x, p_y, p_z (for x, y, z directions) of reinforcement within the element portions.

The stiffness of reinforcement may be characterized, for each integration point, by a (6×6) stiffness matrix $\mathbf{D}^s$ and the total stiffness matrix then becomes

$$\mathbf{D}=\mathbf{D}^c+\mathbf{D}^s.$$

The only non-zero elements of $\mathbf{D}^s$ are

$$\left.\begin{aligned} D_{11}^s &= b_x\,p_x\,E_s,\\ D_{22}^s &= b_y\,p_y\,E_s,\\ D_{33}^s &= b_z\,p_z\,E_s, \end{aligned}\right\} \tag{30}$$

where E_s = tangent modulus of steel (which drops to zero if the bar yields).

Coefficients b_x, b_y, b_z take approximately into account the stiffness contribution of concrete due to bond in the steel. If there are no cracks normal to the bar or if concrete is in compression parallel to the bar, then no correction is needed, i. e., $b_x=1$, or $b_y=1$, or $b_z=1$. If such cracks are present and the steel bar is in tension, concrete between the cracks (in cross-hatched regions, *fig.* 1 *f*) also resists extension, due to bond. Roughly, an annular region of concrete around the bar, having an average diameter d', can be thought to resist the tensile force (*fig.* 1 *f*). Taking $d'\approx 2d$ where d = bar diameter, the stiffness of the annular region is

$$E\,\pi\,[(2\,d)^2-d^2]=3\,E\,\pi\,d^2,$$

while the steel bar stiffness is $E_s\,\pi\,d^2$, giving

$$b_x\sim 1+3\,E\,\pi\,d^2/E_s\,\pi\,d^2=1+3\,E/E_s.$$

The effect of this correction is, however, small; it causes only about 1 % change in maximum moment.

In calculations reported herein, only longitudinal steel has been considered to be continuously distributed. The transverse steel (ties) has been modeled as individual bar elements spanning between the nodes of the grid. This was necessary because the radial force R transmitted at a corner of a tie (*fig.* 1 *g*) into concrete is very important and must be located accurately.

NUMERICAL CALCULATIONS

The matrix equation [equation (8)] that has to be solved at each loading step reads in component form:

$$\begin{bmatrix} \hat{K}_{11} & \hat{K}_{12} & \dots & \hat{K}_{1N} \\ \hat{K}_{21} & \hat{K}_{22} & \dots & \hat{K}_{2N} \\ \hat{K}_{31} & \dots & & \\ \hat{K}_{41} & \dots & & \\ \hat{K}_{51} & \dots & & \\ \dots & & & \\ \hat{K}_{N1} & \dots & & \hat{K}_{NN} \end{bmatrix} \times \begin{Bmatrix} \Delta k \\ \Delta \varepsilon_0 \\ \Delta \gamma_{zx} \\ \Delta v_1 \\ \Delta w_1 \\ \\ \Delta w_n \end{Bmatrix}$$

$$= \begin{Bmatrix} \Delta M + \Delta M'' \\ \Delta N + \Delta N'' \\ \Delta V + \Delta V'' \\ \Delta f_{y_1} + \Delta f''_{y_1} \\ \Delta f_{z_1} + \Delta f''_{z_1} \\ \dots \\ \Delta f_{z_n} + \Delta f''_{z_n} \end{Bmatrix} \tag{31}$$

in which n = number of nodes on one face of the slice, $N = 2n+3$ = number of unknowns, M = cross-sectional bending moment in xz plane, N = axial normal force, V = cross-sectional shear force in z direction, and $\Delta M''$, $\Delta N''$, $\Delta V''$ are the inelastic increments of M, N, V.

We will restrict ourselves to pure bending for which $V = 0$. Then the stress boundary conditions of the slice are

$$\Delta f_{y_1} = \Delta f_{z_1} = \dots = \Delta f_{y_n} = \Delta f_{z_n} = 0,$$

i. e. no forces are actually applied at individual nodes. Then, if ΔM, ΔN and ΔV are specified we can solve for Δk, $\Delta \varepsilon_0$, $\Delta \gamma_{xz}$, Δv_i, Δw_i. However, since we are interested in calculating the strain-softening behavior, we must specify curvature increments instead of ΔM. This is most easily achieved in the same way as displacement boundary conditions are implemented in finite element programs; we replace in equation (31) $\hat{K}_{11}$ with 10^{40} and $(\Delta M + \Delta M'')$ with $10^{40}\, \Delta k_0$, where Δk_0 is the prescribed curvature increment. Since the other terms of the first row in equation (31) are then made negligible in comparison, the solution of the system [equation (31)] will give $\Delta k = \Delta k_0$. To obtain ΔM, we then substitute this solution into the equation given by the original first row of equation (31).

The numerical algorithm within each loading step may be described as follows (where subscripts $r-1$ and r denote the beginning and the end of the step):

1. Evaluate the material properties on the basis of $\boldsymbol{\sigma}_{r-1}, \boldsymbol{\varepsilon}_{r-1}, \xi_{r-1}, \lambda_{r-1}$, etc.; calculate $\Delta \mathbf{S}''$, $\Delta \mathbf{S}''^*$, $\Delta \bar{\mathbf{S}}''$, $\Delta \boldsymbol{\sigma}''$, $\mathbf{C}$, $\bar{\mathbf{C}}$, $\mathbf{D}^c$ and $\mathbf{D}$ for all elements and all integration points (taking $\Delta \boldsymbol{\sigma}'' = 0$ in the first step); and determine finite element stiffness matrix $\mathbf{K}$ as well as the equivalent inelastic nodal force increments $\Delta \mathbf{f}''$ [equation (3)]. (This is in the spirit of forward difference approximation.)

2. Transform the finite element equations to constrained displacements [equations (9)-(11)], solve Δq^* [equation (8)], calculate $\Delta \mathbf{q}$ [equation (5)] and $\Delta \boldsymbol{\varepsilon} = \mathbf{B}\, \Delta \mathbf{q}$ at all integration points of elements, and evaluate $\Delta \boldsymbol{\sigma}^{el} = \mathbf{D}\, \Delta \boldsymbol{\varepsilon}$, $\Delta \boldsymbol{\sigma} = \Delta \boldsymbol{\sigma}^{el} - \Delta \boldsymbol{\sigma}''$ for all these points.

3. Estimate the values of $\boldsymbol{\varepsilon} = \boldsymbol{\varepsilon}_r + \Delta \boldsymbol{\varepsilon}/2$, $\boldsymbol{\sigma} = \boldsymbol{\sigma}_r + \Delta \boldsymbol{\sigma}/2$ for the midstep, and calculate $\Delta \eta$, $\Delta \zeta$, $\Delta \eta'$, $\Delta \zeta'$, $\Delta \lambda$, $\Delta \lambda'$, G, K on the basis of the values of $\boldsymbol{\sigma}$, $\boldsymbol{\varepsilon}$, ξ, η, ζ, etc. for the midstep (central difference approximation). Then evaluate $\Delta \boldsymbol{\sigma}''$ and $\Delta \boldsymbol{\sigma} = \Delta \boldsymbol{\sigma}^{el} - \Delta \boldsymbol{\sigma}''$ using $\Delta \boldsymbol{\sigma}^{el}$ from step 2. Iterate steps 2 and 3 until the values of $\Delta \boldsymbol{\sigma}$ obtained in the new iteration differ negligibly.

4. Calculate the principal stresses and directions at the centroid of each element, check cracking, and if crack formation is indicated record the crack orientation (matrix $\mathbf{R}$) and calculate [similarly as $\Delta f''$ in equation (3)] the nodal forces $\Delta \mathbf{f}^{cr}$ due to $-\sigma^*_{11}$, i.e., due to the release of stress σ^*_{11} that existed before cracking. These nodal forces must be included with $\Delta \mathbf{f}''$ in the next loading step. Then go to step 1 and proceed to analyse the next loading step $(r, r+1)$.

More accurate and more efficient algorithms are no doubt possible, but investigation of various algorithms has been beyond the scope of this project. Note that, to reduce computation cost, the finite element analysis (step 1) is not iterated.

The mathematical model that has been established can be used to analyse a host of practical problems of reinforced concrete: bending ductility of beams and columns, interaction diagrams of columns, effects of ties, stirrups and spirals, effects of load history, stress distribution in compression zone as affected by these parameters, etc. Due to a rather limited scope of this project only a few example cases have been analyzed, with the objective to demonstrate the effect of the stirrups on ductility, a case which can be theoretically treated only with a three-dimensional model. The grid used in numerical examples is shown in figure 1 *b*. Eight-node isoparametric elements have been used.

The calculations have been compared with the test data of Base and Read [1] (for which the reinforcement properties are available in reference [11]) and of Berwanger ([10], [12]), which both document the effect of ties upon ultimate load behavior. A number of other test data exist (e. g., [16], [17], [18], [13], [14], [19], [12], [22], [23]), particularly with respect to axial load-moment interaction or moment-curvature relations, but they were not reported completely enough to allow theoretical comparisons.

The most important effect of the ties on bending is a reduction of strain-softening slope beyond the maximum moment point. This is documented by Base and Read's experimental curves in figure 2 *a* (kip = 4,448 N, in. = 25.4 mm, kip × in. = 113.0 Nm), as well as other data in references [1], [23]. The calculations predicted rather similar behavior; *see* figure 2 *b*, which is based on material parameters from references [3], [5] and represents strictly prediction because no fitting of data by adjusting material parameters has been attempted. (figure 2 *a* pertains to Base and Read's beam No. 8, figure 1 *h*; concrete of strength 4,200 psi, beam 29 days old, mild steel.)

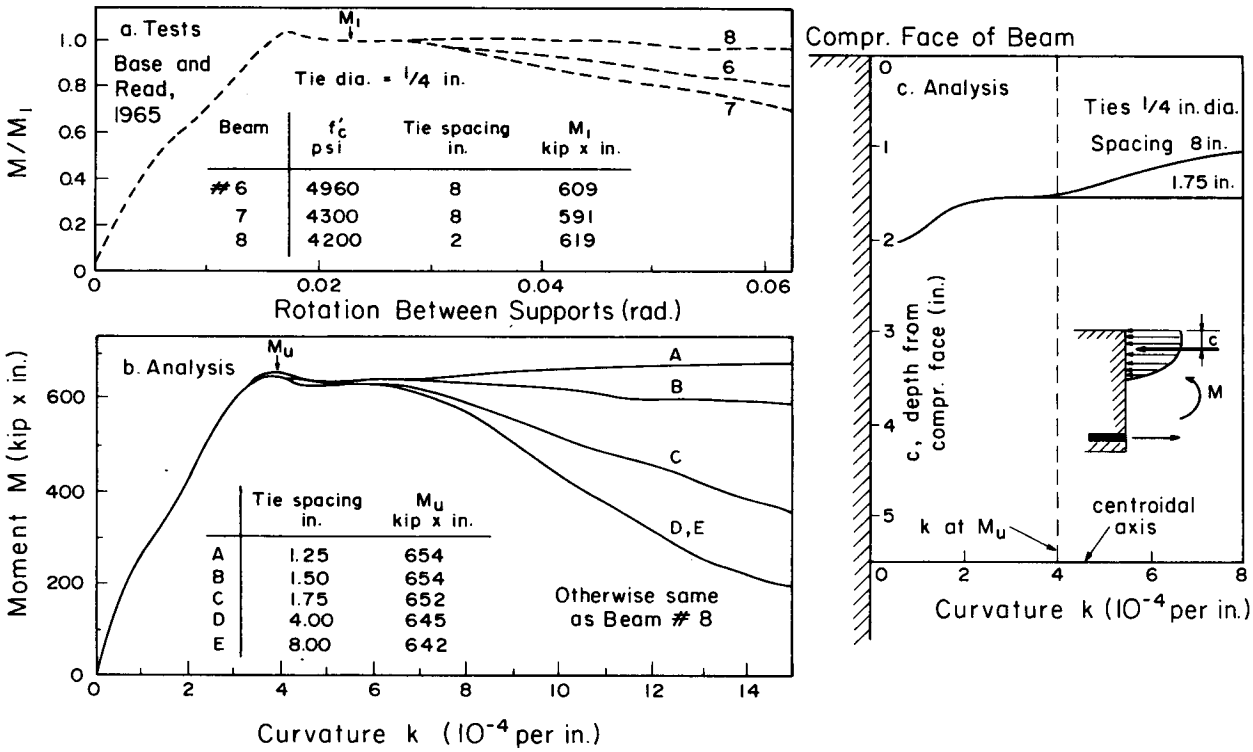

Fig. 2. – Effect of tie spacing on bending ductility (*a*, *b*) and on movement of compression resultant (*c*).

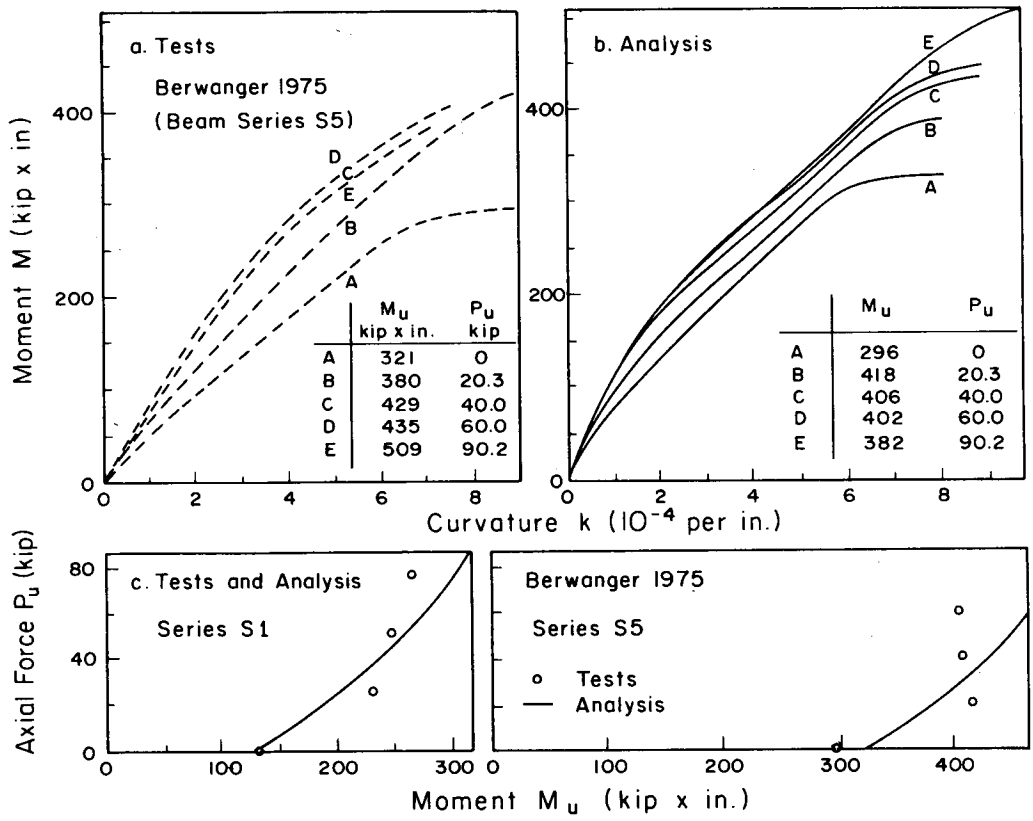

Fig. 3. – Effect of axial load on moment-curvature diagram (*a*, *b*), and ultimate state interaction diagrams (*c*).

Another effect of transverse ties in bending is seen in the compressive stress profile, especially the location of the compression resultant. The profile is known to vary considerably, depending on the ties [19], but precise data are lacking. Computer simulations in figure 2*c* confirm this dependence. When the ties are insufficient, the compression resultant continues to rise after the maximum moment is reached, which causes a sharp drop in the compression resultant and in the bending moment.

Several cases to illustrate the effect of constant axial load on ultimate bending moment have also been predicted; *see* figure 3 showing Berwanger's test results (Berwanger's beam No. 5, 21 days old, of average strength 4,430 psi).

SUMMARY AND CONCLUSIONS

To study the effect of the transverse stress and strain distribution and steel ties (stirrups) upon the ultimate bending moment and bending ductility, a three-dimensional finite element analysis of a cross section slice is carried out. The constraint of planar cross sections allows the results to be interpreted in terms of curvature, bending moment, axial force and shear force. Cracking of concrete is accounted for, the stiffness matrix of inelastic cracked material is derived, and the endochronic theory is used for the constitutive relation of concrete. Numerical examples indicate a satisfactory agreement with available test data on the effect of tie spacing upon the moment-curvature diagrams and ductility.

ACKNOWLEDGMENT

Support by the National Science Foundation under Grant ENG 75-14848-A01 to Northwestern University is gratefully acknowledged.

REFERENCES

[1] Base G. B., Read J. B., *Effectiveness of helical binding in the compression zone of concrete beams*, Journal ACI, Vol. 62, No. 7, July 1965, pp. 763-781.

[2] Bažant Z. P., Bhat D., *Endochronic theory of inelasticity and failure of concrete*. J. of the Eng. Mech. Division, Proc. ASCE, Vol. 102, 1976, pp. 701-722.

[3] Bažant Z. P., Bhat D. B., Shieh C.-L., *Endochronic theory for inelasticity and failure analysis of concrete structures*. Struct. Eng. Report No. 1976-12/259 to Oak Ridge National Laboratory, Northwestern University, Evanston, Ill., December 1976 (available from Nat. Techn. Inf. Service, Springfield, Virginia).

[4] Bažant Z. P., Bhat P., *Prediction of hysteresis of reinforced concrete beams*. Journal of the Struct. Mech. Div., Proc. ASCE, Vol. 103, January 1977, p. 153.

[5] Bažant Z. P., Shieh C.-L., *Endochronic model for nonlinear triaxial behavior of concrete*. Nuclear Engineering and Design, Vol. 47, 1978, pp. 305-315.

[6] Bažant Z. P., *Inelasticity and failure of concrete: A survey of recent progress*. Analisi delle Strutture in Cemento Armato Mediante il Metodo degli Elementi Finiti, Proc., Seminar Commemorating 50th Anniversary of School of Reinf. Concrete, Politecnico di Milano, Milano, June 1978.

[7] Bažant Z. P., *Endochronic inelasticity and incremental plasticity*. Int. J. of Solids and Structures, Vol. 14, 1978, pp. 691-714 (*see* also Addendum II to reference [3]).

[8] Bažant Z. P., Kim S. S., *Plastic fracturing theory for concrete*. Journal of the Engineering Mechanics Division, Proc. Am. Soc. of Civil Engrs., Vol. 105, 1979, pp. 407-428 (and Errata, Vol. 106); *see* also ASCE Meeting Preprint, No. 3431, Chicago, Ill. October 1978.

[9] Bažant Z. P., Shieh C.-L., *Hysteretic fracturing endochronic theory for concrete*. J. of the Eng. Mech. Div., Proc. ASCE, Vol. 106, 1980 (in press); also Structural Engineering Report No. 78-9/640s, Northwestern University, Evanston, Ill., September 1978; *see* also ASCE Meeting Preprint No. 3611, Atlanta, October 1979.

[10] Berwanger C., *Effect of axial load on the moment-curvature relationship of reinforced concrete members*. ACI publication No. SP-50, American Concrete Institute, Detroit, 1975.

[11] *British standard specification for hot rolled bars and hand drawn wire for the reinforcement of concrete*. BS 785, Part 1, 1967, British Standards Institute.

[12] Brown R. E., *Short term axial load-moment interaction characteristics of reinforced concrete members*. ACI Special Publication SP-50, American Concrete Institute, Detroit, 1975.

[13] Cohn M. Z., *Limit design for reinforced concrete structures*. ACI Bibliography No. 8, American Concrete Institute, Detroit, 1975.

[14] Cohn M. Z., Ghosh S. K., *Ductility of reinforced concrete sections in bending*. Inelasticity and Non-Linearity in Structural Concrete, Univ. of Waterloo Press, 1972 (*see* also Publ. Int. Assoc. of Bridge and Struct. Eng., Zürich).

[15] Cook R. D., *Avoidance of parasitic shear in plane element*. Journal of the Structural Division, Proc. ASCE, Vol. 101, ST 6, June 1975, p. 1239.

[16] Hognestad E., *A study of combined bending and axial load in reinforced concrete members*. University of Illinois Engineering Experiment Station, Bulletin Series No. 399, University of Illinois, Urbana, 1951.

[17] Hognestad E., *Inelastic behavior in tests of eccentrically loaded short reinforced concrete columns*. Journal A.C.I., October 1952, Vol. 49, p. 117.

[18] Hognestad E., *High strength bars as concrete reinforcement, Part 2, Control of flexural cracking*. Jnl. Portland Cement Association Res. and Dev. Laboratories, Vol. 7, No. 1, January 1965, p. 42.

[19] Kent C. D., Park R., *Flexural members with confined concrete*. Journal of the Structural Division, Proc. ASCE, July 1971, Vol. 97, ST7, pp. 1969-1990.

[20] Melosh R. J., *Structural analysis of solids*. Journal of the Structural Division, Proc. ASCE, ST4, Vol. 89, August 1963, p. 205.

[21] Ngo D., Scordelis A. C., *Finite element analysis of reinforced concrete beams*. ACI Journal, Vol. 64, March 1967, p. 152.

[22] Park R., Paulay T., *Reinforced concrete structures*. John Wiley and Sons, 1975.

[23] Roy H. E. H., Sozen M. A., *Ductility of concrete*. Proc. of International Symposium on the Flexural Mechanics of Reinforced Concrete, ASCE-ACI, Miami, November 1964, p. 213.

[24] Suidan M., Schnobrich W. C., *Finite element analysis of reinforced concrete*. Journal of the Structural Division, Proc. ASCE, Vol. 99, October 1973, ST10, pp. 2109-2122.

[25] Yuzugullu O., Schnobrich W. C., *A numerical procedure for the determination of the behavior of a shear wall frame system*. ACI Journal, July 1973, Vol. 70, p. 474.

[26] Zienkiewicz O. C., *The finite element method in engineering science*. McGraw-Hill (London), 1971.

RÉSUMÉ

La ductilité en flexion du béton et l'effet de confinement : analyse tridimensionnelle. — *Afin d'étudier les effets de la contrainte transversale et la répartition des déformations ainsi que des armatures d'effort tranchant sur le moment de flexion maximale et la ductilité en flexion, on a entrepris une analyse tridimensionnelle par les éléments finis de la section du segment. Ce segment comprend une couche d'éléments isoparamétriques à 8 nœuds dont les déplacements axiaux sont limités de telle sorte que les sections transversales restent dans le plan mais sans être orthogonales. Cela permet d'interpréter les résultats en termes de courbures, de moments de flexion, de forces axiales et d'efforts tranchants. Chaque élément dans la couche est susceptible de se fissurer indépendamment lorsqu'est dépassée sa résistance en traction limite et l'on établit la matrice de rigidité inélastique croissante du matériau fissuré. Le comportement inélastique du béton non fissuré ou du béton entre les fissures est modellisé selon la théorie endocronique précédemment publiée, qui permet de représenter la dilatance inélastique due au cisaillement, la sensibilité à la pression hydrostatique et la diminution de contrainte à déformation croissante. On se doit d'utiliser une relation de comportement par laquelle on peut décrire ces effets puisque la dilatance du béton est contrecarrée par les ligatures qui déterminent ainsi une pression hydrostatique dans le béton accroissant par là sa ductilité. L'armature transversale est modellisée soit comme une armature répartie de façon continue à travers un élément, soit comme une barre d'acier de connexion entre les nœuds. Des dispositions ont été prises afin d'éliminer les faux effets de contrainte de cisaillement dans le modèle à élément fini. On a rédigé un programme informatique où l'on utilise le processus de chargement croissant pour calculer le diagramme moment / courbure d'une poutre donnée. Les résultats calculés montrent une concordance satisfaisante avec les résultats publiés d'essais réalisés sur l'effet d'espacement des armatures d'effort tranchant sur les diagrammes moment / courbure et la ductilité en flexion.*